Texas A&M University
Mechanical Engineering Department
Turbomachinery laboratory

Parameter Identification of an End Sealed SFD Part I: Identification of Force Coefficients and Operating Conditions Leading to Air Ingestion.

Research Progress Report to the Turbomachinery Research Consortium

TRC-SFD-1-07

Luis San Andrés
Mast-Childs Professor
Principal Investigator

Adolfo Delgado
Research Assistant

May 2007

TRC Project 32513/1519C3

Executive Summary

Open end squeeze film dampers operating with low levels of pressurization are prone to air ingestion and entrapment that drastically reduce their damping capabilities. End seals can significantly reduce the severity of air ingestion. A prior TRC report [3] advances an experimental work to identify the force coefficients of a combined squeeze film damper and mechanical end seal. The test damper configuration includes outlet ports for oil flow through the damper at the sealed end. The system parameters are identified in a two step procedure. First, the mechanical seal friction force is identified from circular orbits tests prior to pumping oil through the damper (i.e. dry system). Second, the squeeze film force coefficients are extracted from the system force coefficients identified from circular orbit tests with oil circulating through the damper.

This report extends the experimental work advanced in [3] to include the identification of force coefficients for the same SFD damper but with closed outlet ports (i.e. no-thru flow). An identification method, suited for non-linear systems, allows to simultaneously identify the squeeze film force coefficients and dry friction force introduced by the mechanical seal. The identification procedure shows similar (within 10 %) damping and added mass coefficients than those reported for the thru-flow configuration. The oil temperature in the squeeze film land does not increase significantly despite the no-thru flow condition. The oil temperature remains constant due to the short length of the experiments, the relatively small amount of energy (work) input into the system, and the large amount of oil stored in the SFD inlet plenum. In an actual application, the no-thru flow condition is expected to lead to an increase of the oil temperature and a significant reduction of damping.

In addition, tests are conducted to find the onset excitation amplitude and frequencies leading to air ingestion. The results, for the maximum allowable shaker loads, demonstrate no evidence of oil cavitation in the damper land. On the other hand, for the largest test amplitude (74 um at 50 Hz) and one of the highest test frequencies (32 um at 100 Hz), the experiments indicate the ingestion of air into the SFD land. Visual observations of the SFD land shows that, besides the seal interface, air is being ingested through other passages including the juncture of the instrumentation facing the damper film land. The amount of air ingested is relatively small and the damper performance is not greatly affected.

Table of Contents

List of Tables

List of Figures

Nomenclature

c	Bearing radial clearance [m]
C_{rv}	Structure remnant damping coefficient [N.s/m]
$C_{s\alpha}$	Structure damping coefficient [N.s/m] $\alpha=x,y$
$C_{s\text{-}\alpha\beta}$	Identified system damping coefficients [N.s/m] $\alpha,\beta=x,y$
$C_{SFD\alpha\beta}$	Identified squeeze film damping coefficients [N.s/m] $\alpha,\beta=x,y$
D	$2\,R$. Damper journal diameter [m]
e	Amplitude or radius of circular centered orbit [m]
$F_{x,y}$	External (shaker) forces applied to bearing [N]
$\overline{F}_x, \overline{F}_y$	Complex components of external forces applied to bearing [N]
F_d	Dry friction force from contact in mechanical seal [N]
f_n	Test system natural frequency [Hz]
$H_{\alpha\beta},L_{\alpha\beta},G_{\alpha\beta}$	Dynamic transfer functions [N/m], $\alpha,\beta=x,y$
K_{sx},K_{sy}	Structural (support) stiffnesses [N/m]
$L,\ R$	Length and radius of SFD land [m]
M_s	Mass of SFD housing [kg]
M_f	Estimated mass of lubricant (feed plenum & end groove) [kg]
$M_{SFD\alpha\beta}$	Squeeze film inertia coefficients [kg], $\alpha,\beta=x,y$
$M_{s\text{-}\alpha\beta}$	Identified system inertia coefficients [kg], $\alpha,\beta=x,y$
M_{plenum}	Oil mass at the SFD inlet plenum [kg]
T	Lubricant temperature [°C]
u,v	Non-linear system inputs [-]
$\overline{u},\overline{v}$	Complex components of model non-linear system inputs [-]
x,y	Bearing dynamic motions along X,Y directions [m]
$\overline{x},\overline{y}$	Complex components of bearing motions [m]
$\dot{x},\dot{y}$	Bearing dynamic velocities along X,Y directions
$Z_{(\omega)}$	Vector of displacements in frequency domain [m]
$\rho,\ \eta$	Lubricant density [kg/m^3] and viscosity [Pa-s]
ω	Excitation frequency [rad/s]

I Introduction

Squeeze film dampers (SFD) aid to reduce synchronous vibration and enhance stability characteristics in rotating machinery. SFDs are prone to air ingestion and lubricant cavitation due to typically low inlet feed pressures. These phenomena are more pervasive with increasing vibration amplitudes and operation frequencies. End sealed SFDs represent an alternative to reduce or retard the occurrence of air ingestion, commonly present in open or partially sealed SFD configurations.

Prior TRC reports [1-3] describe the design and testing of a SFD with an end mechanical seal that replicates a configuration currently in use by one of the TRC members. Prior to this work, no experimental data was available on this type of sealed SFD configuration. The last (2006) TRC report [3] includes flow measurements and dynamic force excitation tests to assess the effectiveness of the end mechanical seal in preventing air entrapment and to identify the force coefficients, respectively. The test configuration includes outlet ports that allow the oil to exit at the sealed end of the damper. The system parameters are identified in a two step procedure. First, the mechanical seal friction force is identified from circular orbits tests prior to pumping oil through the damper (i.e. dry system). Second, the squeeze film force coefficients are extracted from the system force coefficients identified from circular orbit tests with oil circulating through the damper. The test results indicate that the end seal is effective in preventing air ingestion for the range of frequencies and journal displacement amplitudes tested.

This report details experiments to identify the forced coefficients of the mechanically sealed SFD operating with closed outlet ports (i.e. no-thru flow). This configuration is of special interest for unmanned aerial vehicles (UAV). A non-linear identification technique is adopted to identify simultaneously the dry friction force and the squeeze film force coefficients, thus eliminating the need for additional “dry system” tests. The test results are compared to prior test results obtained with thru-flow condition. In addition, the report includes experiments to determine the operating conditions (frequency and amplitude of motion) leading to air entrapment. A literature review of prior experimental work on SFDs relevant to this experimental investigation and non-linear parameter identification techniques follows.

II Literature Review

The 2006 TRC report [3] presents a compilation of the most relevant work related to the present experimental study. Recall that Della Pietra and Adilleta [4,5] present a comprehensive compilation of the experimental and theoretical work conducted on SFDs up to 2002. The following are experimental work publications on SFD since the last report [3] that are pertinent to this research.

Defaye *et al.* [6] present a series of experiments to evaluate the influence of geometric and operating parameters on the force performance of a SFD. The geometric parameters considered include feeding systems (grooves, holes) and their axial location. The operating parameters include lubricant inlet pressure, temperature and journal dynamic eccentricity. The test results show that for a SFD with deep circumferential feed grooves, two independent pressure fields are generated in the squeeze film lands, with a total tangential (damping) force smaller than that generated without a feeding groove. Lubricant cavitation effects are more pronounced at a lower frequency for a SFD with orifice feeding (i.e. no groove). In terms of the operating conditions, high supply pressures delay air ingestion and oil cavitation; while high temperatures (i.e. lower lubricant viscosities) increase the thru flow and diminish the damping capacity of the test SFD.

Adilleta and Della Pietra [7] present measurements of the dynamic pressure field distribution in a squeeze film damper describing off-centered circular orbits. The test conditions include two journal orbit radii (5 % and 25 % of radial clearance), whirling frequencies ranging from 5 Hz-50 Hz, and two lubricant discharge configurations that regulate the amount of air ingested through the damper end. Air ingestion effects are properly characterized by an empirical parameter derived from a physical model developed by Diaz and San Andrés [8]. The dynamic squeeze film pressure waves are displayed for each of the operation conditions. The test results show that lubricant vapor cavitation is more pervasive at lower inlet feed lubricant pressures. In many cases, the cavitation region with lubricant vapor is followed by a short zone with tensile stresses (-0.4 bar). Furthermore, the onset of film rupture due to vapor cavitation only alters the negative region of the dynamic pressure field. This research will be extended to include higher precession frequencies characterizing practical rotordynamic applications.

A review of publications related to parameter identification of non-linear systems from dynamic force excitation tests is of interest. As detailed in the 2006 TRC report [3], the mechanical seal-SFD force response is non-linear due to dry friction interactions at the seal interface. Previously, the system parameters were identified in a two step procedure with the mechanical seal friction force first identified from circular orbits tests prior to pumping oil through the damper (i.e. dry system).

Rice and Fitzpatrick [9] present one the first formal techniques tailored to identify parameters in non-linear mechanical systems using random force excitations. The procedure is based on a cross-spectra frequency analysis to decouple the linear and non-linear force contributions of the mechanical system using residual coherence functions [10]. Non-linear effects are modeled as non-linear inputs with linear operators on a multiple-input/single output transfer function model. The method demonstrates to be robust and computationally light. However, non-Gaussian errors associated to multiple-input/output systems could not be quantified. Thus, a series of tests using different levels of force excitation are needed to validate the identified parameters.

Rouvas *et al.* [11] present the application of spectral density methods to identify linearized force coefficients in fluid film bearings. The test system is excited with impact loads and the bearing force coefficients identified from averaging 200 tests repetitions. The results obtained with power spectral density formulation are similar to those obtained by averaging the data in the time domain, provided that the time data of each repetition is not shifted with respect to each other. The authors validate the use of the power spectral density methods to reduce errors due to signal noise and averaging in the time domain.

Rice and Xu [12] present a general identification method for non-linear systems based on the representation of the system response in terms of the Volterra expansion in the frequency domain. The method employs force excitations with identical frequency spectra at different amplitude levels to decouple the linear and non-linear responses in the frequency domain. The parameters are identified from each decoupled response using a standard least-squares technique. The authors also present an application of the technique to identify the parameters of an insulation material from test data obtained in actual experiments.

Adams *et al.* [13] present a frequency domain technique to simultaneously estimate the linear frequency response matrix and the non-linear parameters of a mechanical

system. The method relies on the principle that the non-linear feedback is directly linked to the spatial nature of the non-linear system. The application of the method is illustrated on two numerical simulations of single or multiple-input/multiple-output SDOF and MDOF systems. The results show the method is effective in determining the linear and non-linear system parameters simultaneously.

Yang *et al.* [14] present a technique for diagnosing vibration using sensitivity functions that are used to correlate the influence of each system parameter over the overall system response. For a SDOF system, these functions are simply defined as the partial derivative of the impedance function with respect to the specific system parameter (i.e. mass, damping, stiffness). The definition of these functions can be extended to MDOF systems. The authors include a practical application of the sensitivity function to locate and eliminate a vibration problem in a vehicle exhaust system.

Yang *et al.* [15] extend the method in [14] for the parameter identification of mechanical systems using sensitivity functions that are expressed in terms of the system transfer functions. The identification procedure involves the linearization of non-linear sources. Although this implies the a-priori knowledge of the non-linear source, the identification procedure can be used to evaluate if the system nonlinearities assumed in the model (i.e. cubic stiffness, quadratic damping, etc.) characterize the system response. The application of the method is illustrated numerically with a 2-DOF system, including an element with a non-linear quadratic stiffness, which is excited with periodic (single frequency) load excitations. The numerical results demonstrate the method effectiveness in determining the degree of freedom in which the nonlinearity is present, and in validating the modeling assumption (i.e. quadratic stiffness).

The present identification method is an adaptation of the Rice and Fitzpatrick [9] method, and also uses definitions from a similar implementation of the method given by San Andrés and Aguilar [16].

III Test Rig Description

Figure 1 depicts a schematic view of the test rig also described in the prior TRC report [3]. Following the same description, the test rig consist of a vertical rigid shaft, mounted on three precision ball bearings (natural frequency 400 Hz [3]), which holds a steel journal of 5” (127 mm) diameter and 3” (76.2 mm) long. The bearing assembly includes two steel plates clamping an acrylic bearing. The two horizontal plates are attached by two vertical steel plates, which also serve as an interface to apply external forces onto the bearing assembly. The top plate includes a lubricant supply connection, a static pressure gauge displaying the feed pressure into the bearing and four eddy current sensors facing the shaft. The composite bearing housing hangs from a top structure with four steel rods providing structural stiffness to the test bearing section. A mechanism atop of the test rig, comprising two sliding flat plates (top and bottom support plates), allows adjusting the position of the bearing center with respect to the shaft to simulate centered and off-centered operation conditions.

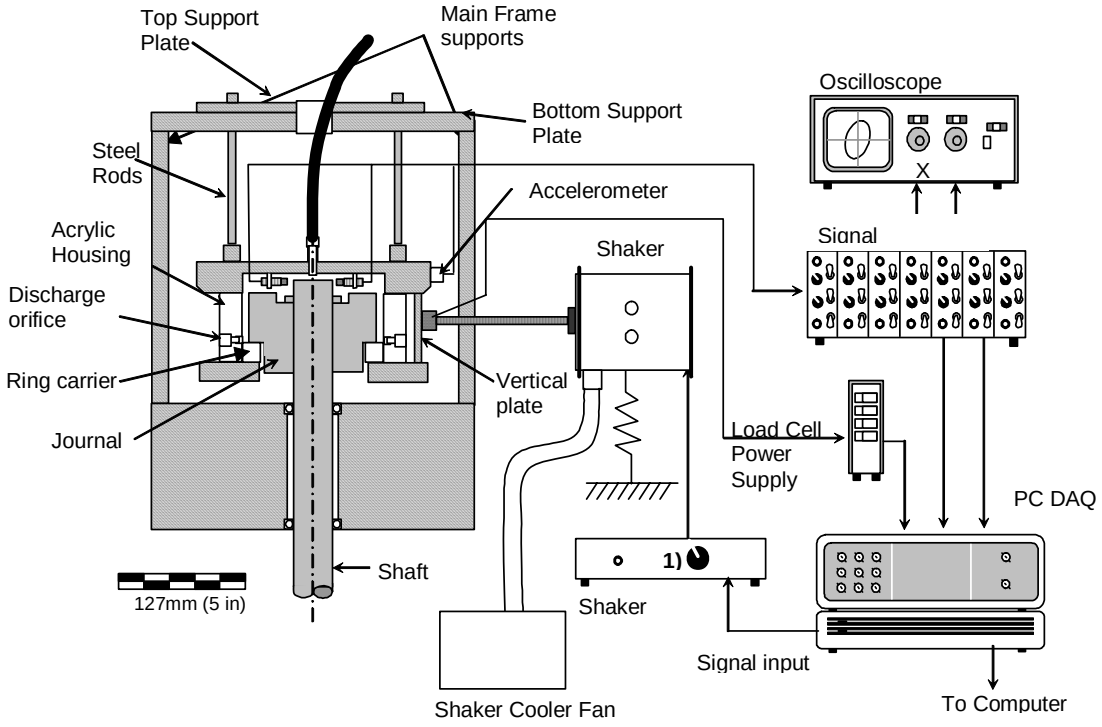

Figure 1 Test rig for dynamic force measurements and flow visualization in a sealed end SFD

The bearing housing design integrates a SFD land and an annulus that accommodates a metallic ring (ring carrier). A wave spring pushes the ring holder against the journal and

provides a contact force between the matting surfaces to seal the damper. Figure 2 and 3 depict a cross section and a cut view of the end sealed SFD design along with its components, respectively. The configuration tested in [3] included four outlet ports at the discharge groove that allowed flow of the oil across the damper. In the current test set up these ports are sealed (i.e. no thru flow allowed).

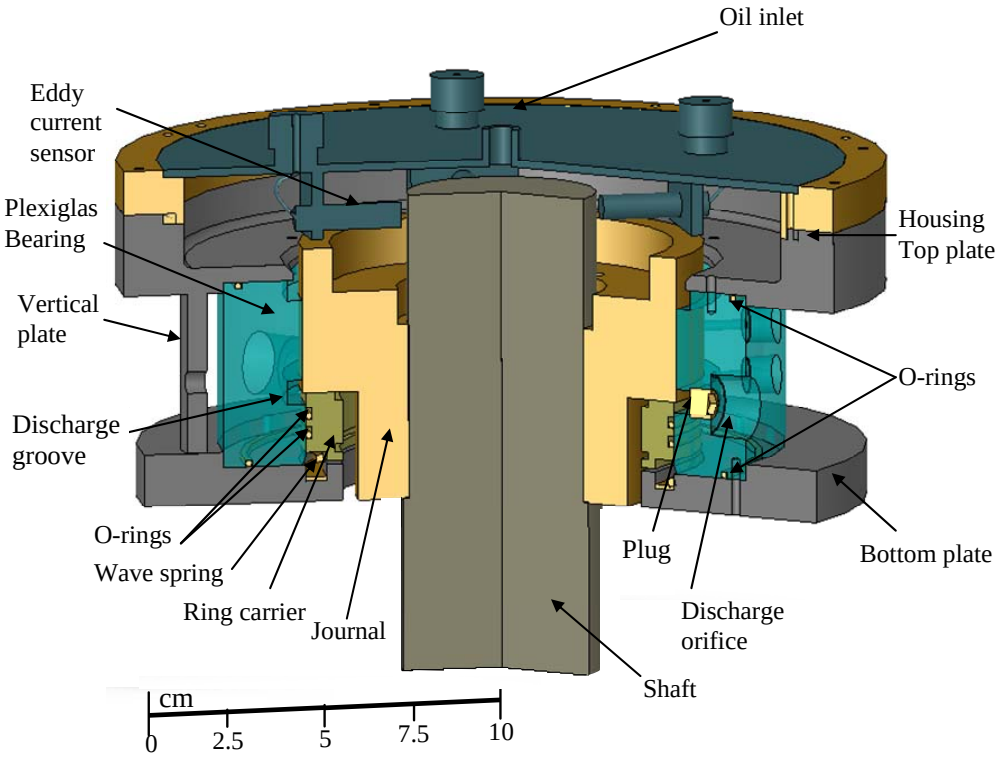

Figure 2 Sealed-end SFD assembly cross section view.

Figure 4 shows the instrumentation arrangement and the reference coordinate system on the SFD housing. The instrumentation consists of two accelerometers, four Eddy current sensors and two load cells. The system is excited via two electromagnetic shakers suspended from separate steel structures (90 degrees apart). Slender stingers connect the electromagnetic shakers to the piezoelectric load cells attached to vertical plates on the bearing housing. A customized data acquisition system records all the sensor signals and controls the electromagnetic shakers.

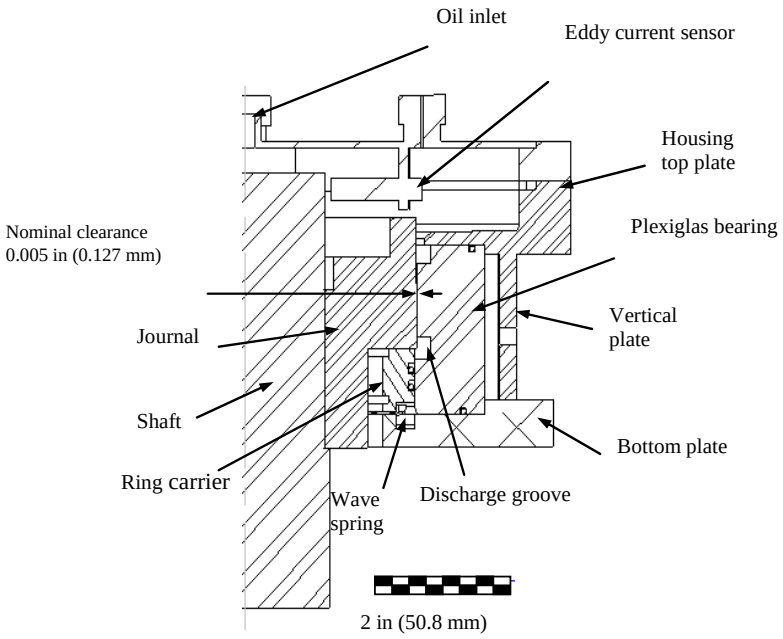

Figure 3 Sealed-end SFD assembly cut view.

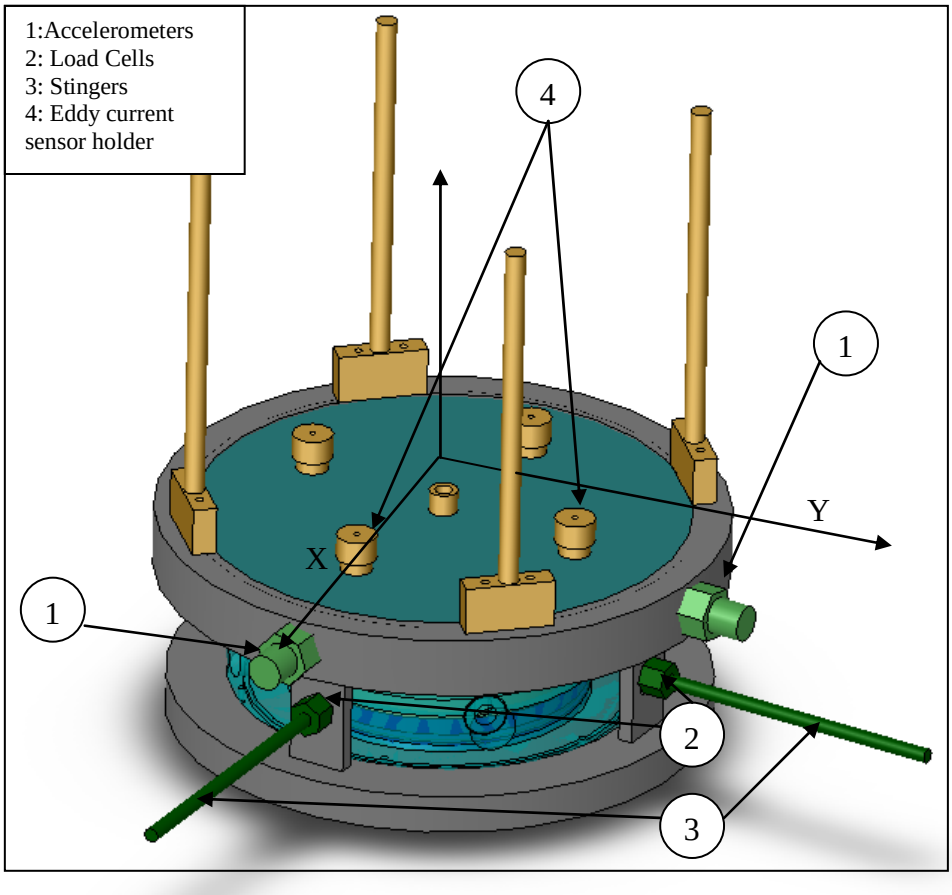

Figure 4 SFD housing reference coordinate system and location of sensors.

IV Parameter identification

IV.1 Experimental procedure

The system is excited with single frequency loads ensuing circular centered orbits of the test element. The tests include four motion amplitudes (25 μm to 50 μm) at frequencies ranging from 20 Hz to 70 Hz. The excitation load amplitudes are adjusted throughout the test frequency range to maintain constant amplitude circular orbits (25 μm, 31μm, 38 μm, 50 μm). The tests conditions are similar to those in Ref. [3] to allow direct comparisons of the end results. Table 1 presents the test conditions and lubricant properties. Figures 5 and 6 show the recorded displacement orbits for two selected frequencies (20 and 60 Hz).

Table 1 Test conditions for dynamic load tests (CCO). Lubricated SFD

Inlet Pressure (P_s)*	31 kPa
Discharge groove pressure (P_r)*	8.6 kPa-15.5 kPa
Frequency Range	20-70 Hz (5 Hz step)
Lubricant temperature (T)	23-25 ^{0}C (73-77 ^{0}F)
Viscosity (η)	3.1 cP- 2.8 cP
Clearance (c)	125-127 μm (4.9-5 mil)
Orbit amplitude (e)	25-50 μm (1-2 mil)

*: Gauge pressure. **: no thru-flow.

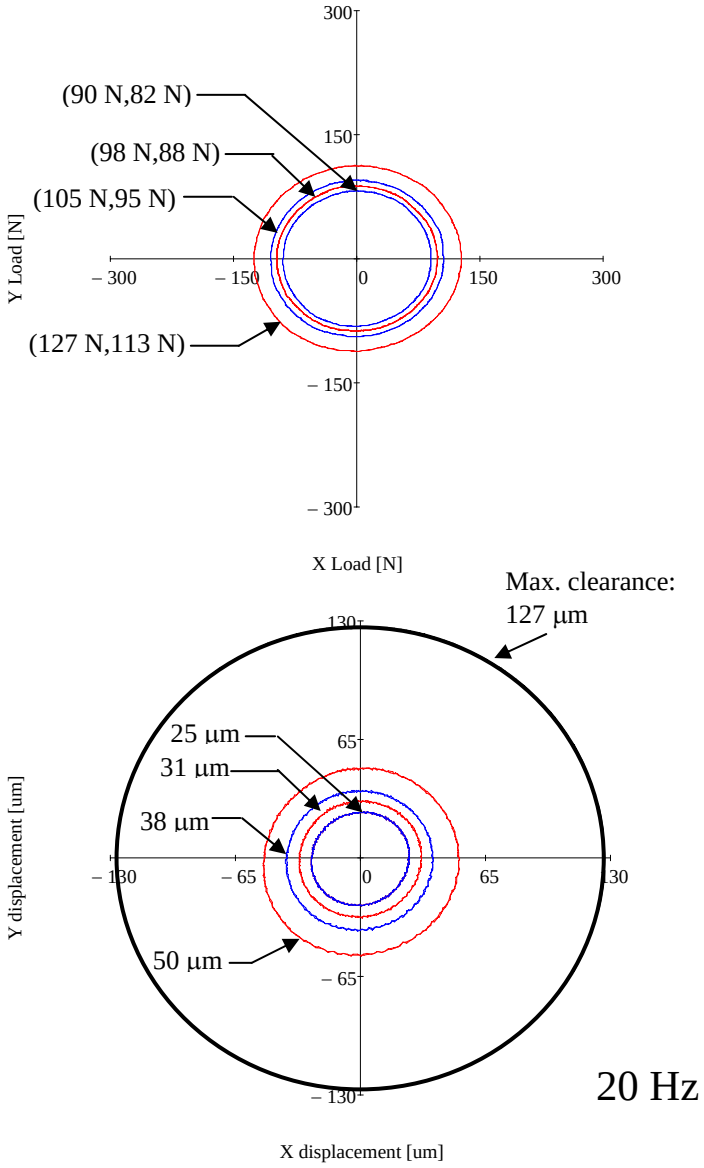

Figure 5 Recorded load and ensuing displacement orbits for four amplitude load magnitudes. Clearance circle noted. (20 Hz, lubricated SFD, CCO)

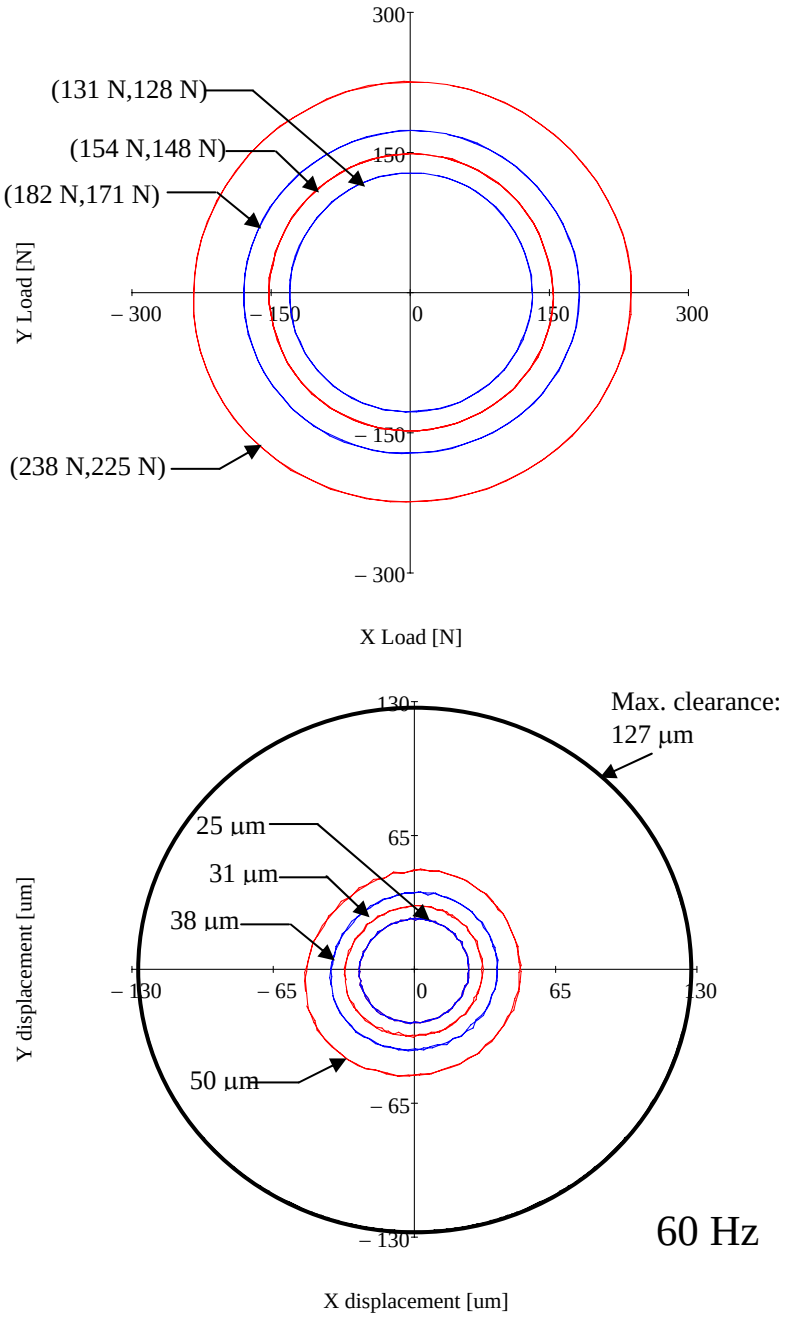

Figure 6 Recorded load and ensuing displacement orbits for four amplitude load magnitudes. Clearance circle noted. (60 Hz, lubricated SFD, CCO)

IV.2 Identification method

The seal-SFD force parameters are identified from circular centered orbits using an adaptation of the methods presented in Refs. [9,16] using single frequency dynamic load excitations. Figure 7 shows a schematic view of the equivalent mechanical system representation of the SFD with mechanical seal.

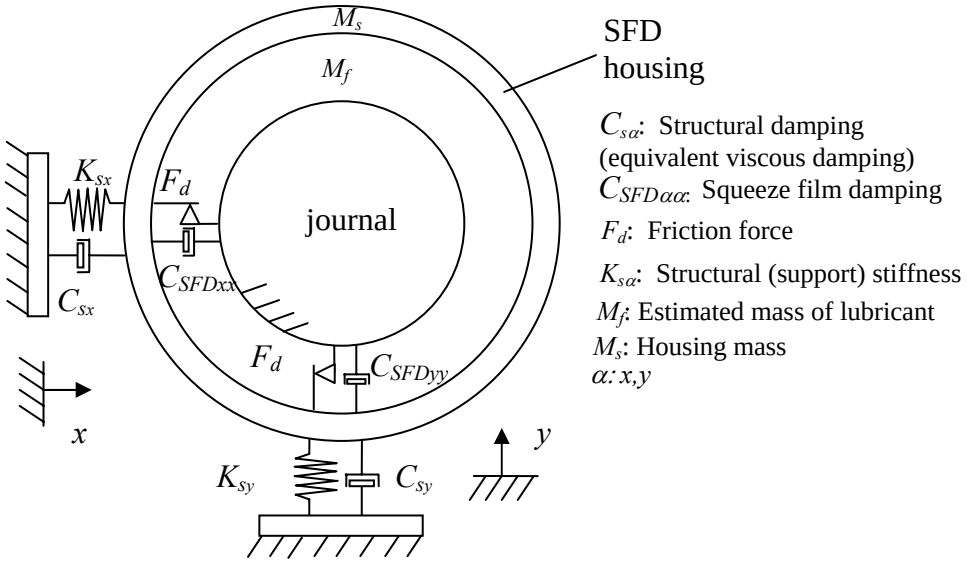

Figure 7 Schematic view of the equivalent representation of the SFD with mechanical seal

The equations of motion for the test bearing section are [3]

$$\begin{bmatrix} M_s + M_f & 0 \\ 0 & M_s + M_f \end{bmatrix} \begin{Bmatrix} \ddot{x} \\ \ddot{y} \end{Bmatrix} + \begin{Bmatrix} C_{sx}\dot{x} \\ C_{sy}\dot{y} \end{Bmatrix} + \begin{Bmatrix} K_{sx}x \\ K_{sy}y \end{Bmatrix} = \begin{Bmatrix} F_x \\ F_y \end{Bmatrix} - \begin{Bmatrix} F_x \\ F_y \end{Bmatrix}_{seal} - \begin{Bmatrix} F_x \\ F_y \end{Bmatrix}_{SFD} \tag{1}$$

where M_f is the mass of fluid enclosed in the plenum above the fluid film land section and in the discharge groove. $(C_s)_{x,y}$ are the equivalent viscous damping coefficients that characterize the damping arising from the structural support. These coefficients, obtained from impact tests on the dry structure [3], equal 230 N.s/m.

The SFD linearized reaction forces are

$$\begin{Bmatrix} F_x \\ F_y \end{Bmatrix}_{SFD} = \begin{bmatrix} C_{SFD_{xx}} & 0 \\ 0 & C_{SFD_{yy}} \end{bmatrix} \begin{Bmatrix} \dot{x} \\ \dot{y} \end{Bmatrix} + \begin{bmatrix} M_{SFD_{xx}} & 0 \\ 0 & M_{SFD_{yy}} \end{bmatrix} \begin{Bmatrix} \ddot{x} \\ \ddot{y} \end{Bmatrix} \tag{2}$$

where $\{C_{SFD\alpha\beta}\}_{\alpha\beta=x,y}$ $\{M_{SFD\alpha\beta}\}_{\alpha\beta=x,y}$ are the damping and inertia force coefficients, respectively. As demonstrated in a prior report [3], cross-coupled force coefficients are negligible since the damper operates without oil cavitation.

The seal dry friction (non-linear) force is expressed as [16]

$$\begin{Bmatrix} F_x \\ F_y \end{Bmatrix}_{seal} = F_d \begin{Bmatrix} \dot{x} \\ \dot{y} \end{Bmatrix} \frac{1}{\sqrt{\dot{x}^2 + \dot{y}^2}} = F_d \begin{Bmatrix} u \\ v \end{Bmatrix} \tag{3}$$

where F_d is the friction force amplitude and $u,v= \{\dot{x},\dot{y}\}/\sqrt{\dot{x}^2+\dot{y}^2}$ are the non-linear input paths to the system, and derived from two original inputs (x and y) in the time domain[1]. Thus, the system is represented as a four-input/two output equivalent model shown in Figure 8, where D is the time derivative operator.

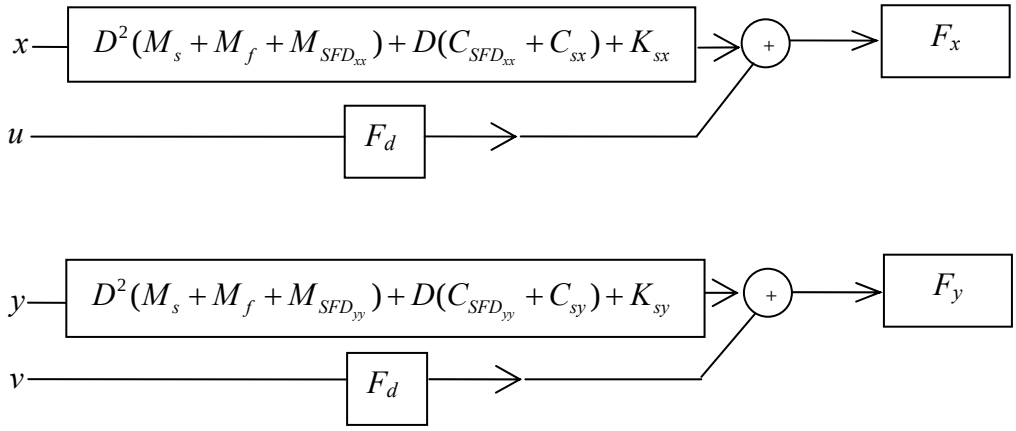

Figure 8 Elements of a four-input/two output representation of the non-linear mechanical seal-SFD system [16]

Periodic single frequency load excitations are represented as

$$F_x(t)=F_{xc}\cos(\omega t)+F_{xs}\sin(\omega t)=\left(F_{xc}-iF_{xs}\right)e^{i\omega t}=\bar{F}_x e^{i\omega t}$$
$$F_y(t)=F_{yc}\cos(\omega t)+F_{ys}\sin(\omega t)=\left(F_{yc}-iF_{ys}\right)e^{i\omega t}=\bar{F}_y e^{i\omega t} \quad (4)$$

and the ensuing bearing displacement and accelerations for the model linear path inputs (i.e. x and y) are also periodic with identical frequency (ω), and expressed as

$$Z_{(\omega)}=\begin{Bmatrix}x\\y\end{Bmatrix}=\begin{Bmatrix}x_c-ix_s\\y_c-iy_s\end{Bmatrix}e^{i\omega t}=\begin{Bmatrix}\bar{x}\\\bar{y}\end{Bmatrix}e^{i\omega t};\ \begin{Bmatrix}\ddot{x}\\\ddot{y}\end{Bmatrix}=\begin{Bmatrix}\bar{a}_x\\\bar{a}_y\end{Bmatrix}e^{i\omega t} \quad (5)$$

In the frequency domain the system is represented as

[1] Recall that in the experiments, the excitation forces are the actual inputs and the displacements (x,y) and modeled non-linear inputs (u, v) represent the outputs of the system.

$$\bar{F}_x = L_{xx}\bar{x} + F_d\bar{u}\ ;\ \ L_{xx} = \left(K_{s_x} - \omega^2 M_{s-xx} + i\omega C_{s-xx}\right)$$
$$\bar{F}_y = L_{yy}\bar{y} + F_d\bar{v}\ ;\ \ L_{yy} = \left(K_{s_y} - \omega^2 M_{s-yy} + i\omega C_{s-yy}\right) \qquad (6)$$

where

$$M_{s-xx} = M_{SFD_{xx}} + M_f + M;\ M_{s-yy} = M_{SFD_{yy}} + M_f + M;$$
$$C_{s-xx} = C_{SFD_{xx}} + C_{sx};\ C_{s-yy} = C_{SFD_{yy}} + C_{sy}; \qquad (7)$$

and $(\bar{x}, \bar{y})$, $(\bar{F}_x, \bar{F}_y)$ are the discrete Fourier Transform (DFT) of time varying displacements and forces, respectively. L_{xx}, L_{yy} are the linear transfer functions containing the stiffness, inertia and damping coefficients. $(\bar{u}, \bar{v})$ represent the DFT of the model non-linear inputs $(\{\dot{x}, \dot{y}\}^T / \sqrt{\dot{x}^2 + \dot{y}^2})$, obtained by building the velocity vector $(\dot{x}, \dot{y})^T$ constructed using the Fourier coefficients of the displacement (x_c, x_s). This procedure effectively reduces signal noise.

The dry friction force (F_d) can be identified from Eq.(6) using two single frequency force excitations with different amplitude levels provided that the force coefficients in Eq. (7) are independent of the vibration amplitude. However, this is not the case for the SFD since, as theory predicts and experimental results demonstrate [3], damping coefficients are a function of the amplitude of journal motion. This dependency of the damping coefficient on the vibration amplitude is assumed to be linear for small differences is amplitudes, as shown in previous experimental work [3]. Thus, the squeeze film damping forces are represented in the general form $C_{SFDxx} = a_x|\bar{x}| + b_x$ and $C_{SFDyy} = a_y|\bar{y}| + b_y$, with $a_{x,y}$ and $b_{x,y}$ as generic constants. For multiple excitation load levels

$$H_{xx}{}^i = \left(K_{s_x} - \omega^2 M_{s-xx} + i\omega C_{sx}\right) + i\omega(a_x|\bar{x}^i| + b_x) + F_d G_{xx}{}^i$$
$$H_{yy}{}^i = \left(K_{s_y} - \omega^2 M_{s-yy} + i\omega C_{sy}\right) + i\omega(a_y|\bar{y}^i| + b_y) + F_d G_{yy}{}^i;\ \ i = 1...N \qquad (8)$$

with

$$H_{xx}{}^{i} = \frac{\bar{F}_x^{\,i}}{\bar{x}^i}; \quad G_{xx}{}^{i} = \frac{\bar{u}^i}{\bar{x}^i}$$
$$H_{yy}{}^{i} = \frac{\bar{F}_y^{\,i}}{\bar{y}^i}; \quad G_{yy}{}^{i} = \frac{\bar{v}^i}{\bar{y}^i} \tag{9}$$

where N is number of independent load excitations. The friction force is identified from three load excitations inducing three different orbit amplitudes

$$F_d = \frac{H_{\alpha\alpha}{}^{1} + H_{\alpha\alpha}{}^{3} - 2H_{\alpha\alpha}{}^{2}}{G_{\alpha\alpha}{}^{1} + G_{\alpha\alpha}{}^{3} - 2G_{\alpha\alpha}{}^{2}}; \quad \alpha : x, y \tag{10}$$

with the superscripts (1,2,3) representing independent test with different excitation amplitudes. Note that the displacement differences are constant (i.e. $\left|\bar{x}^1\right| - \left|\bar{x}^2\right| = \left|\bar{x}^2\right| - \left|\bar{x}^3\right|$; $\left|\bar{x}^1\right| - \left|\bar{x}^2\right| \approx 0.05c$)

Once the friction force is identified, it can be used directly for any other excitation amplitude without any restrictions on orbit amplitude level since the friction force is only a function of the seal assembly force (i.e. normal force). The parameters from the linear transfer functions (L_{xx},L_{yy}) are obtained from least square fits of their real and imaginary parts, i.e.

$$\begin{aligned} K_{s_x} - \omega^2 M_{s-xx} &= \mathrm{Re}(L_{xx}) = \mathrm{Re}(H_{xx} - F_d G_{xx}) \\ \left(\omega C_{s-xx}\right) &= \mathrm{Im}(L_{xx}) = \mathrm{Im}(H_{xx} - F_d G_{xx}) \\ K_{s_y} - \omega^2 M_{s-yy} &= \mathrm{Re}(L_{yy}) = \mathrm{Re}(H_{yy} - F_d G_{yy}) \\ \left(\omega C_{s-yy}\right) &= \mathrm{Im}(L_{yy}) = \mathrm{Im}(H_{yy} - F_d G_{yy}) \end{aligned} \tag{11}$$

The squeeze film added mass and damping and damping coefficients are then extracted from

$$\begin{aligned} M_{SFDxx} &= M_{s-xx} - M_s - M_f \\ M_{SFDyy} &= M_{s-yy} - M_s - M_f \end{aligned}; \quad \begin{aligned} C_{SFDxx} &= C_{s-xx} - C_{sx} \\ C_{SFDyy} &= C_{s-yy} - C_{sy} \end{aligned} \tag{12}$$

IV.3 Results: Dynamic force coefficients

This section presents the identified force coefficients for the no thru-flow configuration and compares them to coefficients obtained for the previous test

configurations including open outlets at the discharge groove (i.e. with thru-flow). Figure 9 depicts the dry friction force (F_d) identified from the procedure outlined above. The results also include the dry friction coefficient (F_d=53 N) identified, as in prior reports, from dry system tests (i.e. with no lubricant). Appendix A details the experimental procedure to obtain the dry friction force from dry system tests. The test results show good correlation between both methods, with the current F_d being ~2% larger than that identified via energy methods and in a lengthier two step procedure. Furthermore, the friction force remains fairly constant throughout the test frequency range.

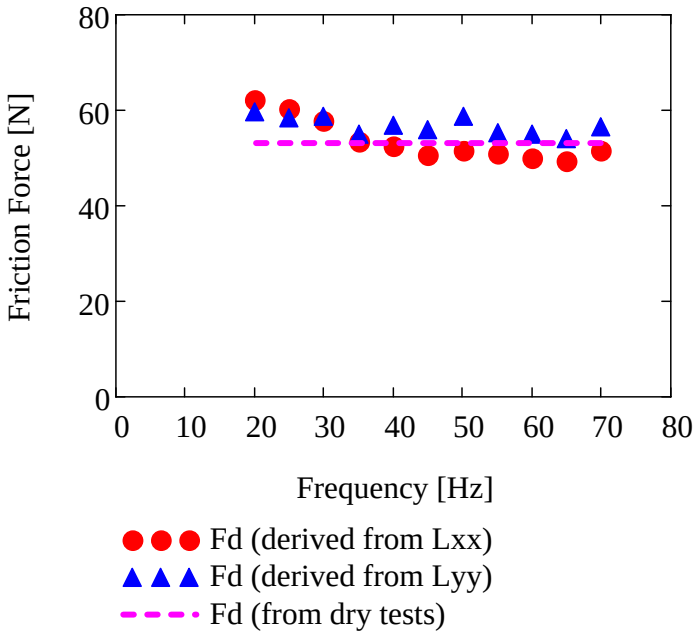

Figure 9 Dry friction force identified from circular centered orbits. Dotted line represents dry friction estimated from energy method and tests under dry conditions.

Figure 10 shows, for the largest amplitude of orbital motion (50 μm), the real part of the linear path transfer function (L_{xx}, L_{yy}) and the corresponding curve fit. Table 2 presents the identified values of added mass coefficients and the average identified dry friction force. The added mass results are similar to those obtained in the prior report [3] for the thru-flow configurations (within 15 %). The present results, just like the previous ones, show large values of added mass coefficients (i.e. half the system mass) and evidence the importance of fluid inertia effects in SFDs.

Table 2 SFD inertia coefficients and dry friction force identified from circular centered orbit tests (frequency range 20-70 Hz, no thru-flow)

Parameter	***xx***	***yy***
Friction Fore (F_d) (average)	**54 N**	
System Mass, (M_s)	**20.2 kg**	**20.6kg**
Squeeze film inertia (M_{SFD})	**9.9 kg**	**10.3 kg**
r^2 (goodness of curve fit)	0.99	0.98
Fluid Mass, (M_f) [kg]	0.62	

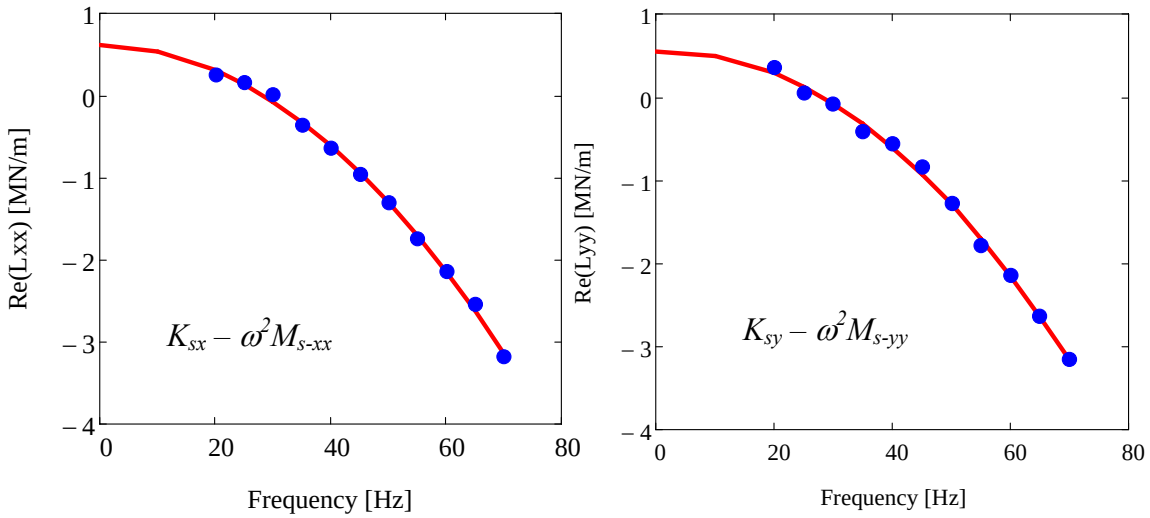

Figure 10 Real part of dynamic stiffnesses versus frequency. Circular centered orbits of amplitude *x,y*: 50 μm (K_{sx}= 853 kN/m, K_{sy}= 885 kN/m.)

Figure 11 shows the imaginary part of the linear transfer function (L_{xx}, L_{yy}) and the corresponding curve fit ($\omega C_{SFDxx,yy}$) for the largest amplitude of motion (50 μm). The slope of the curve fit represents the squeeze film damping coefficients (C_{SFDxx}, C_{SFDyy}). The goodness (r^2=0.99) of the curve fits using ($\omega C_{SFDxx,yy}$) indicates that the dry friction damping contribution has been effectively subtracted from the system overall damping. The results show larger (by ~13 %) damping coefficients in the *x* direction than in the *y* direction.

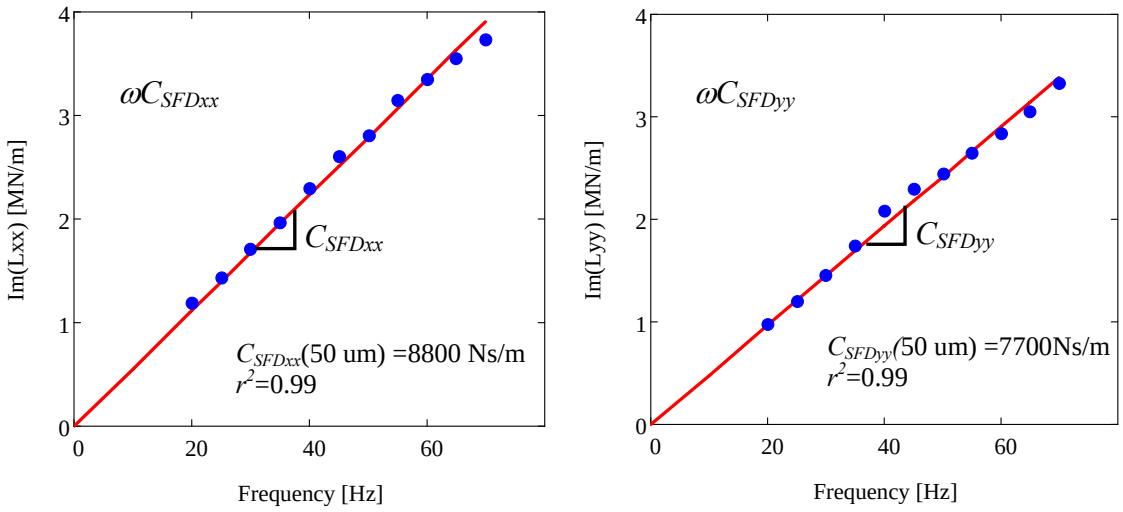

Figure 11 Imaginary part of linear impedance function versus excitation frequency. (C_{SFDxx}) Circular centered orbits of amplitude *x,y*: 50 μm (no thru-flow)

Figure 12 shows the squeeze film damping coefficient (C_{SFDyy}) versus orbit amplitude. The figure also includes the coefficient (C_{SFDyy}) obtained from the thru-flow configuration using 2.8 mm flow restrictors [3], an improved damping prediction for small motions about a centered condition [17], and predictions based on the short length bearing model [18]. The error bars denote the uncertainty associated to each coefficient following the uncertainty analysis detailed in Ref. [19]. The damping increases for increasing orbit amplitudes as in the previous test configuration. Furthermore, the current damping coefficient is slightly larger (~10 %) but within the uncertainty of that reported for the thru-flow configuration using the 2.8 mm flow restrictors. Thus the damper operating with no thru-flow is also effective. The improved damping prediction for centered conditions (from Ref. [17]) is within the uncertainty values of the damping coefficient identified for the smallest orbit amplitude. These experimental results are of interest in applications that need fully sealed dampers and can contain the oil within the damper land for extended periods of time (i.e. UAV application).

Note, however, that the current test results correspond to laboratory tests maintaining a relatively constant temperature, ~ 2 ^{0}C variation at SFD land and oil plenum (see Table 1). The temperatures are maintained constant throughout the experiments due to their short duration (~ 30 min), the low level of energy input into the system (maximum power 5.7 W- average work 3.1 kJ) and the large mass of oil (0.59 kg) in the inlet plenum above the damper land that together with other system components account for a thermal

capacity of 4.1 kJ. In actual applications, with no-thru flow and with a limited volume of oil, it would be necessary to consider the increase of oil temperature and the corresponding viscosity reduction when estimating the system damping performance.

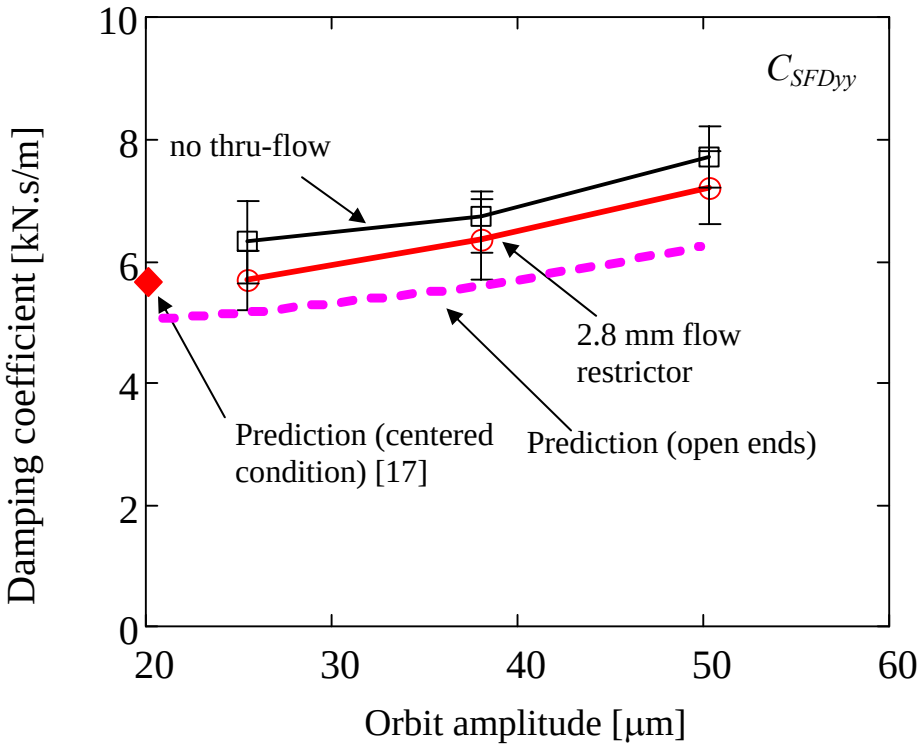

Figure 12 Squeeze film damping coefficient (C_{SFDyy}) versus orbit amplitude. (Circular Centered Orbits, No thru-flow, flow restrictor: 2.8 mm [3])

Figure 13 depicts the identified system and squeeze film damping coefficient versus excitation frequency. The system damping coefficient, which includes the equivalent action of dry friction, is frequency dependent and notably larger than the extracted squeeze film damping coefficient. Also notice that the system damping is larger for the smallest amplitude (i.e. 25 μm). These characteristics are distinctive of a system with dry friction [3]. On the other hand, the squeeze film damping coefficients are independent of the frequency, and largest for the largest amplitude tested (i.e. 50 μm). These results indicate that the identification method is effective in discerning the squeeze film damping contribution from the overall system damping.

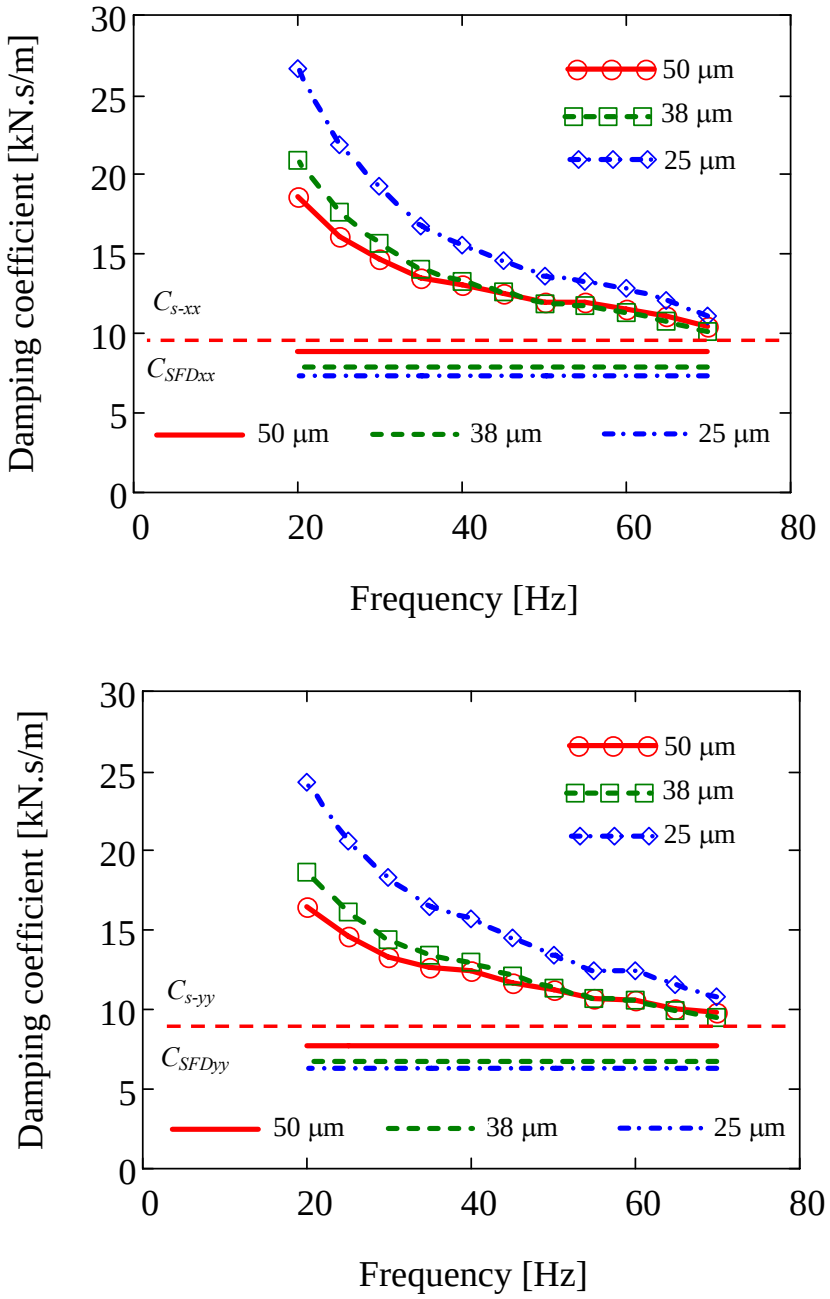

Figure 13 Squeeze film damping coefficients (C_{SFDxx}, C_{SFDyy}) and system damping coefficients ($C_{s\text{-}xx}$,$C_{s\text{-}yy}$) versus excitation frequency for increasing orbit amplitudes. (Circular Centered Orbits, No thru-flow)

V Onset amplitude and frequency leading to air ingestion and lubricant cavitation in test SFD

This section presents results from single frequency load excitation experiments conducted on the SFD test rig with closed outlet ports (i.e. no thru-flow). The static pressure at the inlet plenum and the discharge groove are 3 psia (31 kPa). Periodic loads excite the SFD inducing circular centered orbits with radii ranging from 31 μm to 74 μm (i.e. from 25% to 60% of radial clearance). The experiments serve to identify the limit orbital motion amplitudes for onset of air ingestion and lubricant cavitation. Table 3 summarizes the test conditions.

Table 3 Test conditions for dynamic load tests (CCO). Lubricated SFD. No thru-flow.

Inlet pressure (P_s)*	31 kPa
Discharge groove pressure (P_r)*	31 kPa
Frequency range	20-120 Hz (5 Hz step)
Lubricant temperature (T)	25 ^{0}C-26 ^{0}C (76 ^{0}F-79 ^{0}F)
Viscosity (η)	3.1 cP- 2.8 cP
Clearance (c)	125-127 μm (4.9-5 mils)
Orbit amplitude (e)	31-69 μm (1.2-2.7 mils)
Flow restrictors (hole diameter)	No thru-flow.

*: Gauge pressure.

V.1 Experimental procedure

Single frequency dynamic loads excite the test system with constant circular orbit amplitudes for the given range of frequencies (5, 10 Hz increments). The test maximum frequency for each orbit amplitude is limited by the shaker maximum force. Specifically, the experiments are halted once the shakers output force reaches 80% (360 N) of their maximum capacity (445 N). For the smallest orbit amplitude tested (32 μm) the system was excited up to 110 Hz, and up to 50 Hz for the largest amplitude tested (74 μm).

Figures 14 through 16 depict the excitation forces and corresponding damper orbits for 32 μm, 50 μm and 74 μm at the highest frequency tested for each amplitude level (i.e. 110 Hz, 90 Hz and 50 Hz), respectively. Figures 13 and 15 show a fairly circular load and circular bearing orbits. Figure 14 shows a more elliptical orbit for the excitation load and response orbit of 50 μm. The ellipticity may be attributed to the structural orthotropy of

the system (K_{sx}= 853 kN/m, K_{sy}= 885 kN/m) that becomes more evident for large amplitude of motions.

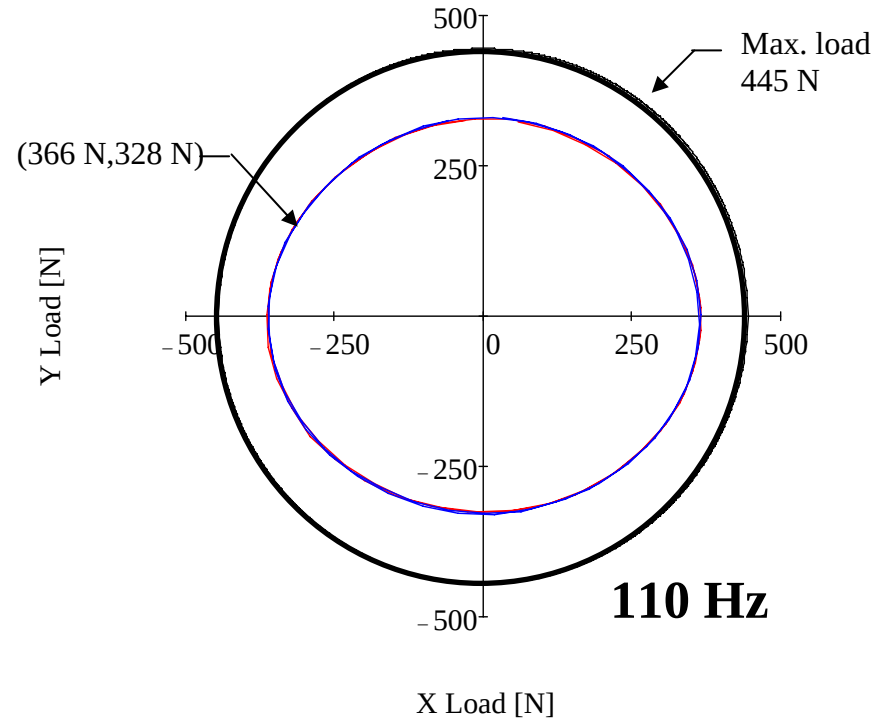

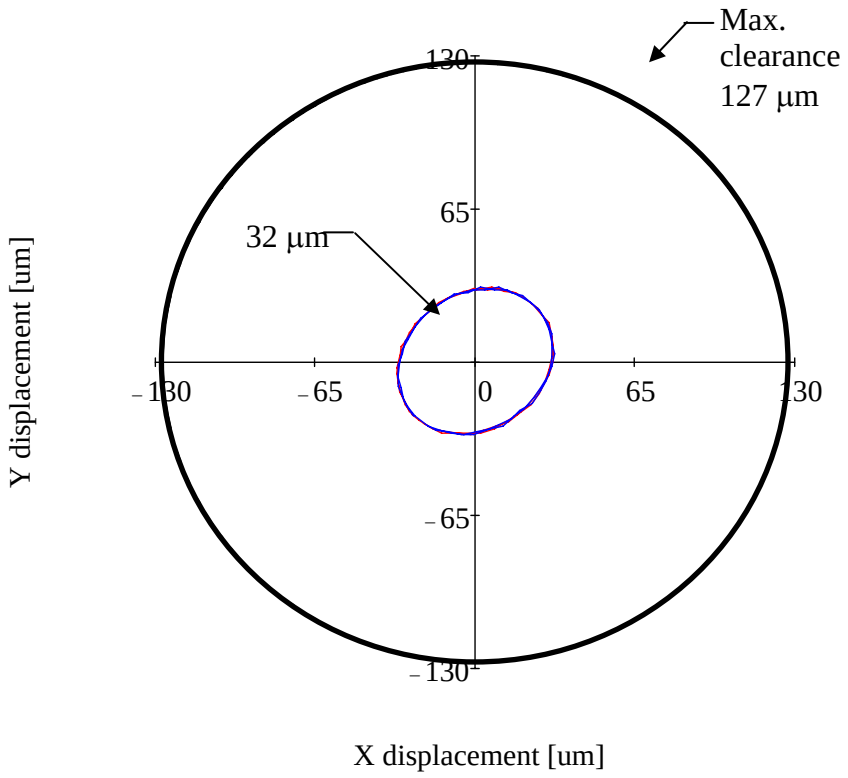

Figure 14 Excitation load and response orbits (motion) from experimental data. (110 Hz, Load: [N], displacement [μm], 32 μm)

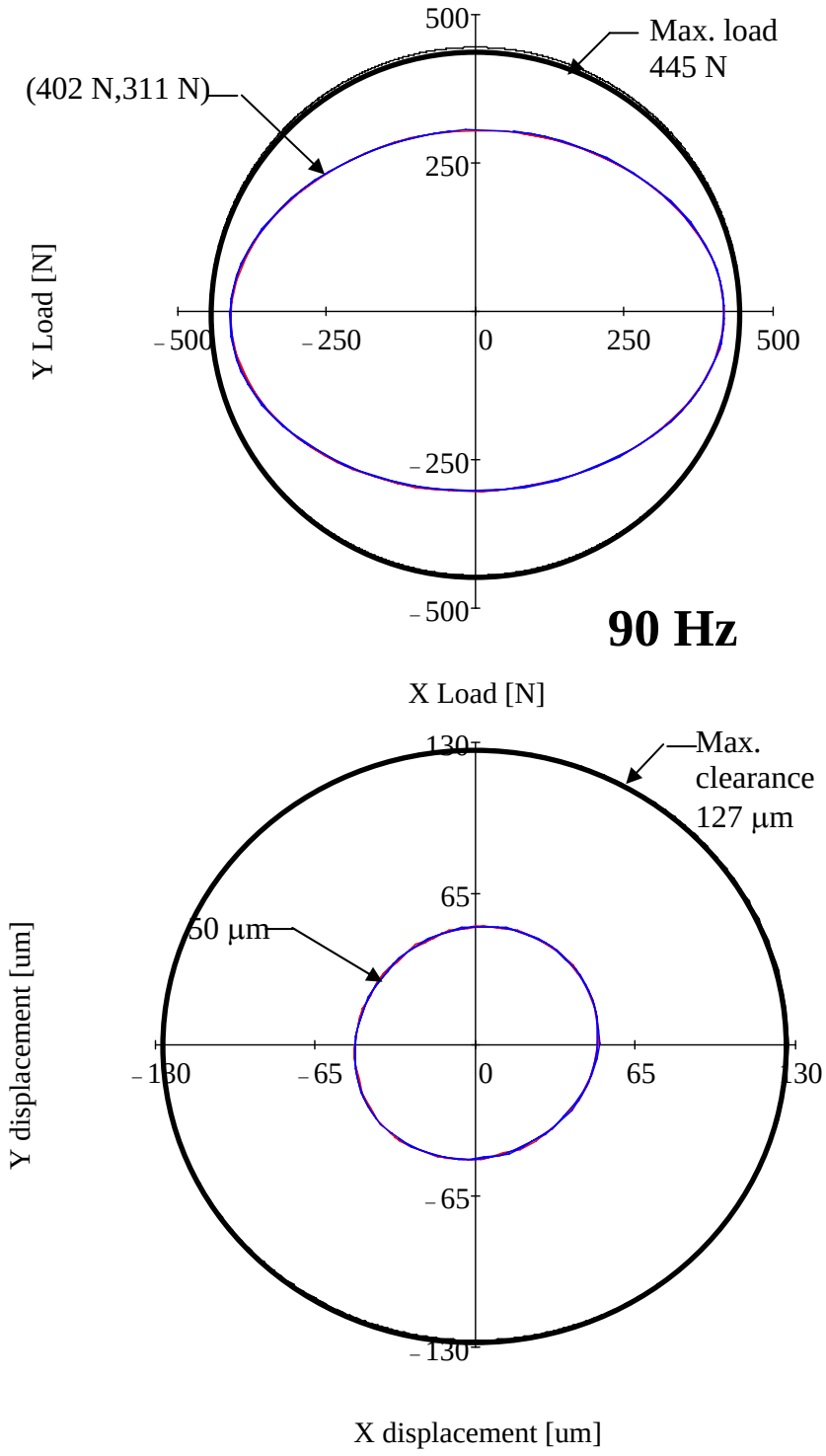

Figure 15 Excitation load and response orbits (motion) from experimental data. (90 Hz, Load: [N], displacement [μm], 50 μm)

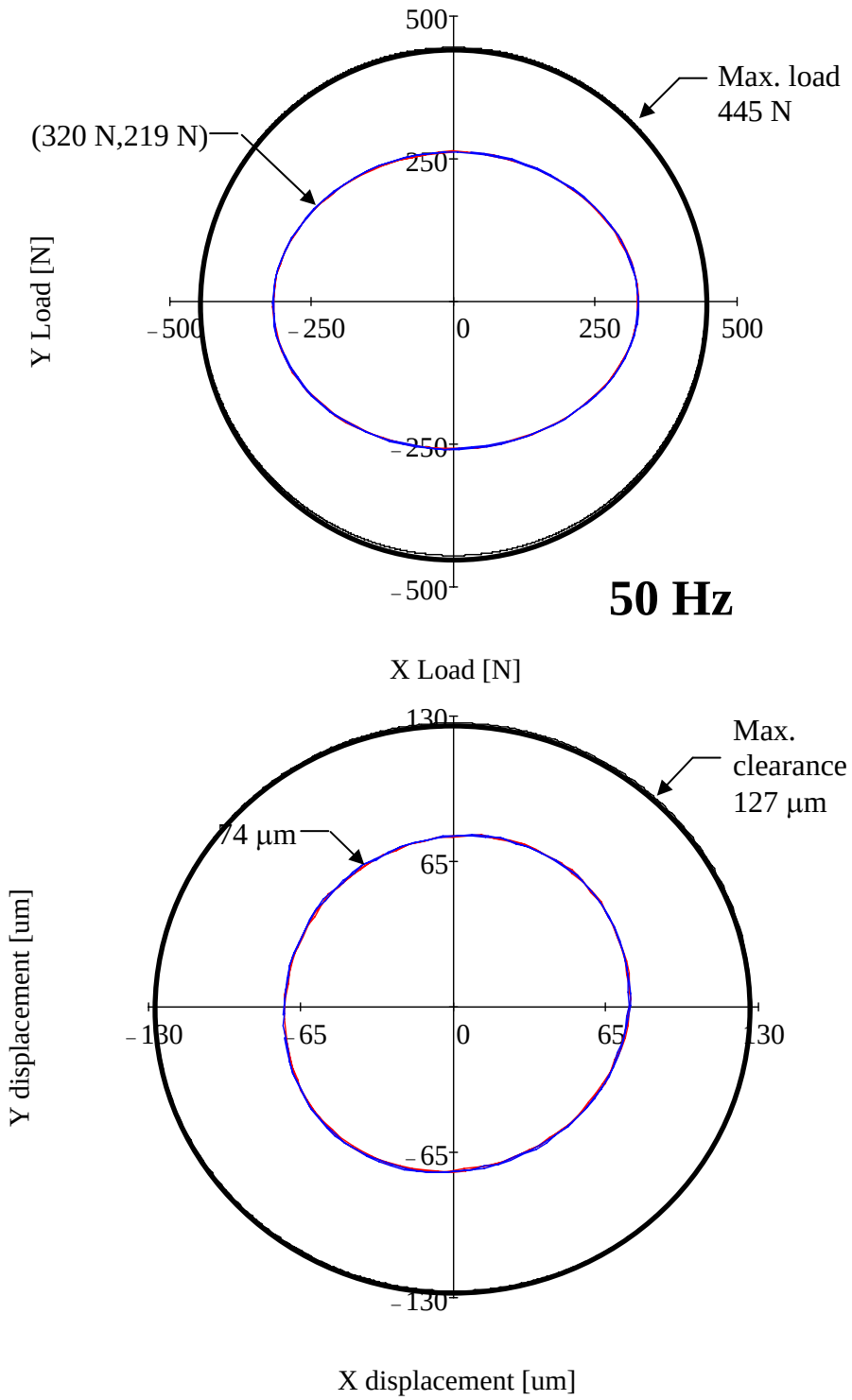

Figure 16 Excitation load and response orbits (motion) from experimental data. (50 Hz, Load: [N], displacement [μm], 74 μm)

V.2 Experimental Results

Figure 17 shows the location of the dynamic pressure sensors. The two sensors are located at the mid-span of the SFD land and discharge groove, respectively.

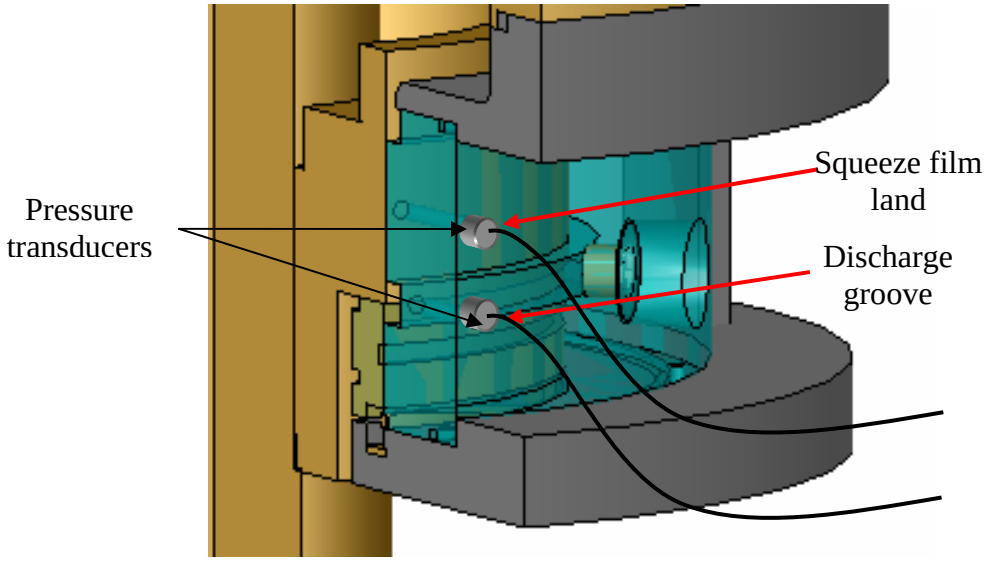

Figure 17 Cut view of SFD housing detailing the location of pressure sensors

The presence of air in the squeeze film land is evaluated by examining the peak-to-peak pressures and the actual dynamic pressure waves. The presence air bubbles in the damper land is associated with a decrease of the peak-to-peak dynamic pressure [20]. Air ingestion and formation of bubbles can also be identified from the shape of the dynamic pressure wave. The presence of air bubbles in the damper land produces a flat pressure zone between the minimum and maximum pressure peaks. The length of this flat portion in the dynamic pressure wave is an indicative of the severity of air ingestion [20]. On the other hand, the deformation (flattening) of the low pressure peak is an indicative of oil vapor cavitation [7,20,21].

Figure 18 shows the peak-to-peak values of the dynamic pressure at the squeeze film land (c=127 μm). The peak pressures steadily increase with frequency and amplitude of orbital motion. Furthermore, the film pressure shows a linear dependency on the excitation frequency with a constant slope for most of the test conditions. However, for the lowest amplitude tested (32 um) the dynamic pressure significantly deviates from the linear pattern (i.e. reduction of the slope) for frequencies above 90 Hz. Thus, at such operating conditions, it is likely the occurrence of oil cavitation or air entrapment into the

damper film land. This can be further corroborated by examining the shape of the dynamic pressure waves.

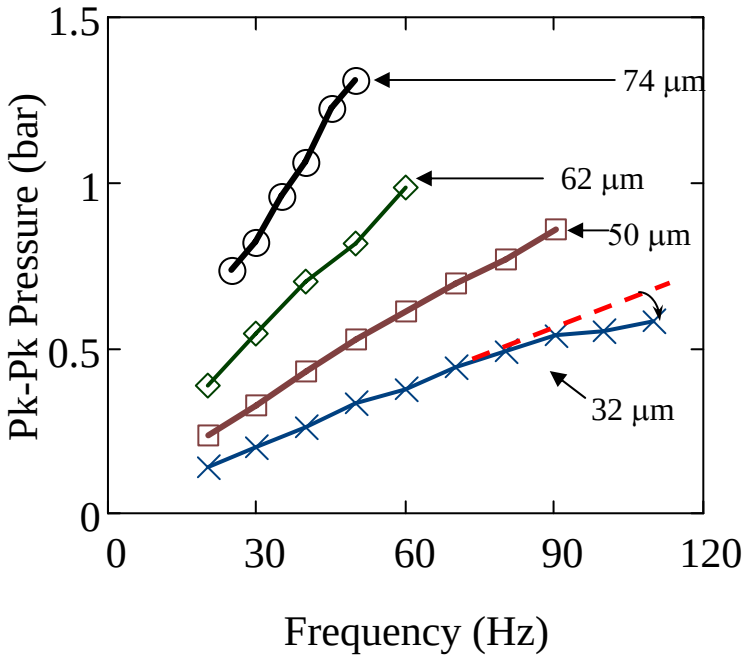

Figure 18 Peak-peak dynamic pressures in squeeze film land versus frequency and various orbit amplitudes.

Figure 19 displays the peak-to-peak dynamic pressure recorded at the discharge groove. The peak pressure remains nearly constant for frequencies up to 60 Hz, then increases as the excitation frequency increases. The pressure at the discharge groove represents around 30 % of the pressure measured at the land for the smaller excitation amplitude tested. For the lowest test frequency, the formation of the dynamic pressure at the groove rapidly increases with frequency, and becomes comparable (up to 60 % for 32 μm orbits) to the values of pressure generated in the film land.

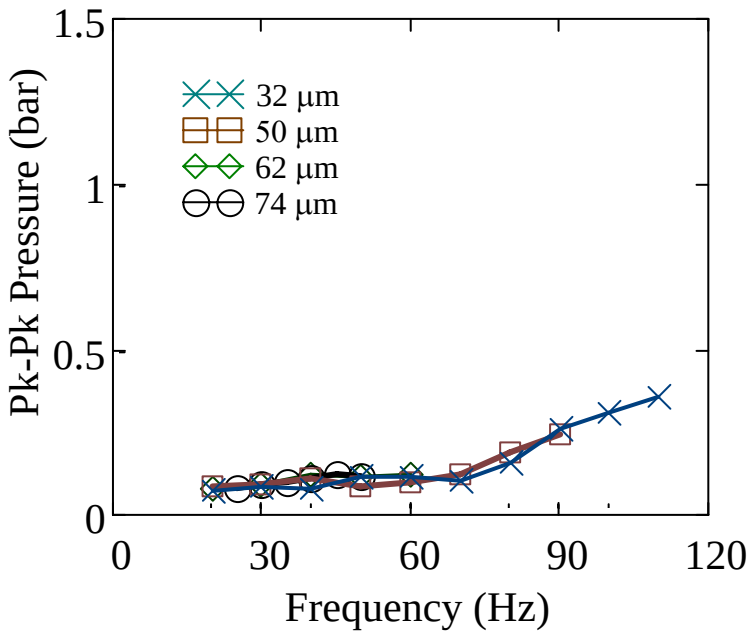

Figure 19 Peak-peak dynamic pressures in discharge groove versus frequency and various orbit amplitudes.

Figures 20 through 23 show the dynamic pressure waves at the squeeze film land and discharge groove for all the amplitude orbits (32 μm, 50 μm, 62 μm, 74 μm) at the highest test frequencies. None of the figures shows evidence of oil cavitation (i.e. minimum peak pressure is not altered). In addition, there is not strong evidence of air ingestion for the 50 μm and 62 μm orbit amplitudes at the maximum test frequencies (see Figures 21 and 22). On the other hand, Figures 20 and 23 show the formation of a flat portion (uniform pressure) in the dynamic pressure wave between the transition from minimum to maximum pressure, thus indicating the presence of air in the damper film land [20]. Visual observations of the squeeze film land at such operating conditions evidence the presence of small air bubbles at both operating conditions (Figures 20 and 23). Although, it is possible that air is being ingested through the seal interface, visual inspection of the damper land during operation also suggests that air is ingested through different passages such as the juncture of the temperature and pressure sensors and the Plexiglas housing (see Figure 24). In addition, the severity of air ingestion is rather mild considering the short length of the flat region in between the peaks of the dynamic

pressure[2]. Thus, the damper performance is not severely affected at such operating conditions.

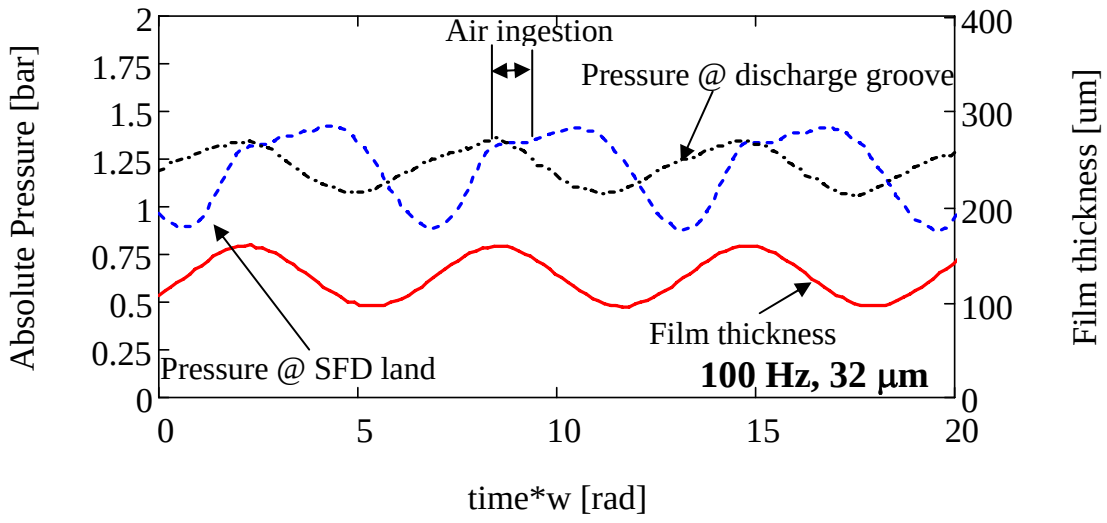

Figure 20 Dynamic pressure measurements at SFD land and discharge groove (including film thickness at sensor location). (100 Hz, 32 μm orbit amplitude, supply pressure= 31 kPa, no thru-flow)

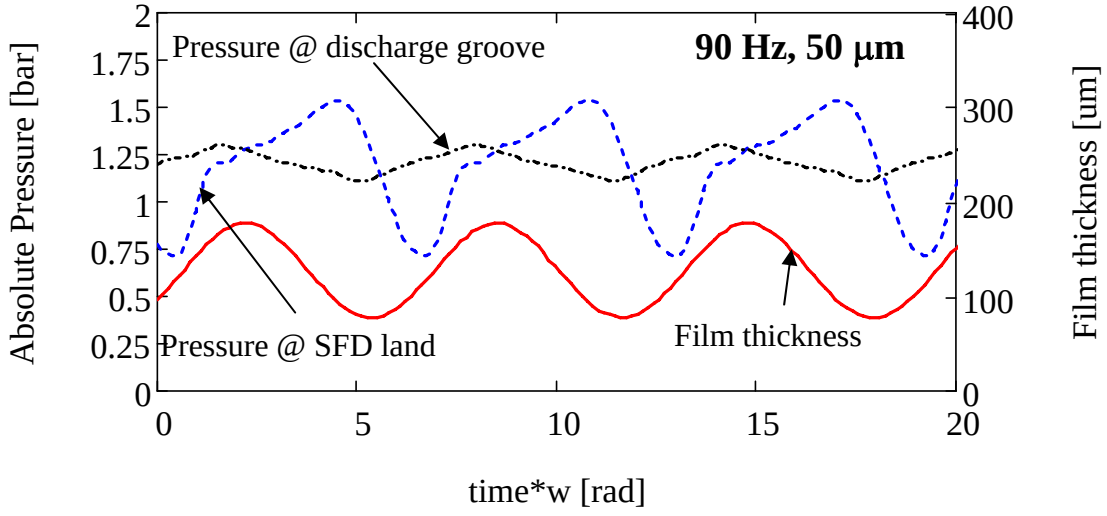

Figure 21 Dynamic pressure measurements at SFD land and discharge groove (including film thickness at sensor location). (90 Hz, 50 μm orbit amplitude, supply pressure= 31 kPa, no thru-flow)

[2] Digital videos of different levels of air ingestion and corresponding squeeze film pressure waves are shown in the Tribology group website (http://phn.tamu.edu/TRIBGroup) [22].

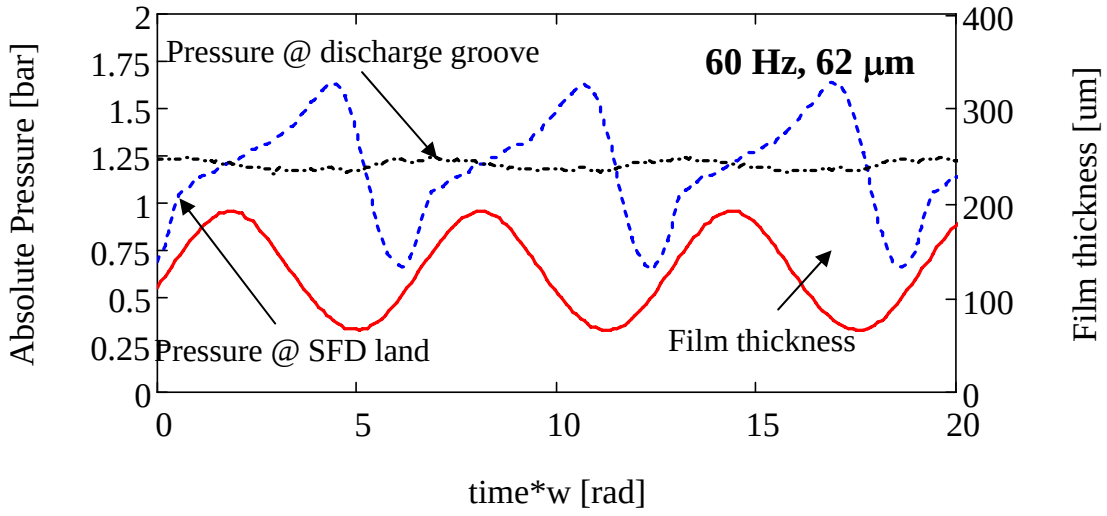

Figure 22 Dynamic pressure measurements at SFD land and discharge groove (including film thickness at sensor location). (60 Hz, 62 μm orbit amplitude, supply pressure= 31 kPa, no thru-flow)

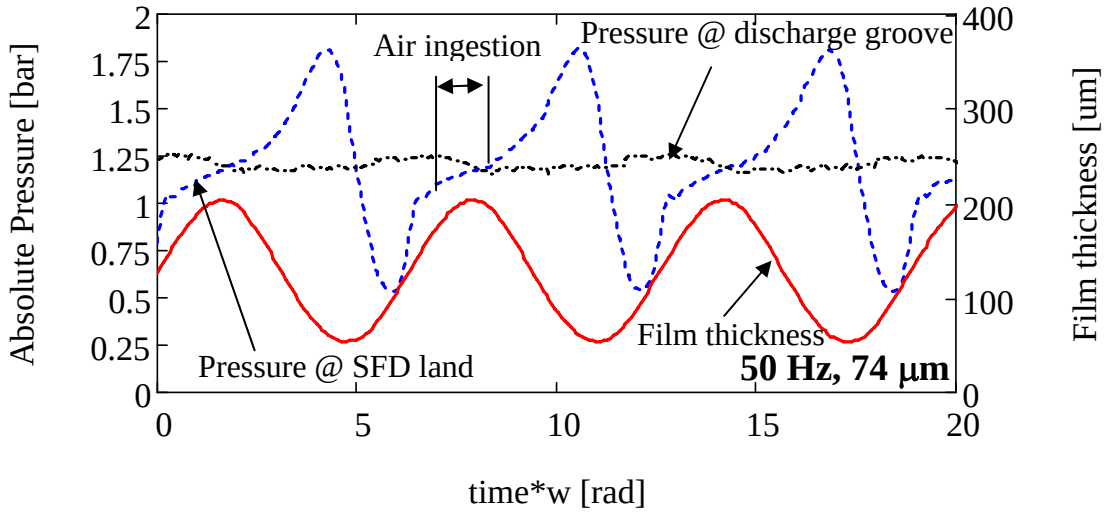

Figure 23 Dynamic pressure measurements at SFD land and discharge groove (including film thickness at sensor location). (50 Hz, 74 μm orbit amplitude, supply pressure= 31 kPa, no thru-flow)

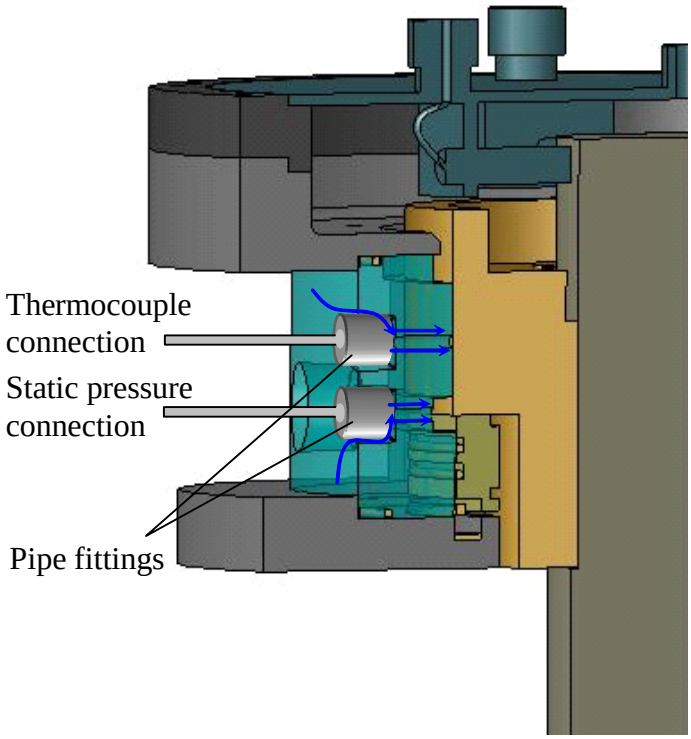

Figure 24 Cut view of SFD showing likely paths for air ingestion.

VI Conclusions and Recommendations

This report describes the identification of force coefficients in a SFD with a mechanical seal and evaluates the effectiveness of the seal in preventing air ingestion. The damper discharge ports are closed so there is no thru-flow. An identification method is implemented to simultaneously identify the squeeze film force coefficients and the friction force from the mechanical seal. The squeeze film damping coefficients are accurately identified from a curve fit of the linear path transfer function Im(L_{xx} L_{yy}), which evidences the effectiveness of the method in determining the non-linear vicious-like damping contribution of the mechanical seal.

The damper added mass coefficients are similar to those reported for the thru-flow configuration. The damper damping coefficients are a function of the orbital amplitude and similar (10 % larger) to those reported for the damper thru-flow configuration. The oil temperature remains relatively constant throughout the experiments despite there is no-thru lubricant flow. The temperature equilibrium during the tests is associated to the small duration of the tests, the small amount of work input into the system, and the large amount of oil residing in the inlet plenum. In an actual application, i.e. damper operating with no thru-flow, the oil will heat up and the damping capacity will be greatly affected.

In addition, tests are conducted to find the onset excitation amplitude and frequencies leading to air ingestion. The results, for the maximum allowable loads, demonstrate no evidence of oil cavitation in the damper film land. On the other hand, for the largest test amplitude (74 um at 50 Hz) and the highest test frequency (32 um at 110 Hz), pressure measurements indicate the ingestion of air into the squeeze film land. Besides the seal interface, visual observation evidences the ingestion of air through passages like the juncture of the instrumentation facing the squeeze film land and discharge groove. However, the severity of the air ingestion is relatively small for the test excitation amplitudes and frequencies.

The test results demonstrate that the damper is effective in avoiding air ingestion and its damping performance is not greatly affected. Thus, the SFD with closed outlet ports (i.e. no thru-flow) is a viable option for a UAV application. However, damping predictions should be accompanied with a thermal analysis based on the geometric configuration and operating conditions to predict the temperature variation of the oil. In addition, further tests have to be conducted to simulate other operation conditions like

non-circular and off-centered orbits, for example. Also, tests need to be conducted for larger contact forces at the seal interface and to evaluate their impact in the SFD performance.

Future work will include tests with multiple frequency excitations to simulate actual operating conditions in multi-spool engines. The identification method will be extended to obtain the force coefficients from eccentric journal orbits with multiple frequencies.

VII References

[1] Delgado, A., and San Andrés, L., 2004, "Sealed end Squeeze Film Damper: Test rig Description and Identification of Structural Parameters," TRC report, TRC-SFD-1-04, May.

[2] Delgado, A., and San Andrés, L., 2005, "Identification of Force Coefficients in a Squeeze Film Damper with a Mechanical Seal," TRC report, TRC-SFD-1-05, May.

[3] Delgado, A., and San Andrés, L., 2006, "Identification of Force Coefficients in a Squeeze Film Damper with a Mechanical Seal," TRC report, TRC-SFD-1-06, May.

[4] Della Pietra, L., and Adiletta, G., 2002,"The Squeeze Film Damper over Four Decades of Investigations. Part I: Characteristics and Operating Features," Shock Vib. Dig, **34**(1), pp. 3-26.

[5] Della Pietra, L., and Adiletta, G., 2002,"The Squeeze Film Damper over Four Decades of Investigations. Part II: Rotordynamic Analyses with Rigid and Flexible Rotors," Shock Vib. Dig., **34**(2), pp. 97-126.

[6] Defaye, C., Arghir, M., Carpentier, P., Bonneau, O., Debailleux, C., and Imbourg, F., 2005 "Experimental Investigation of the Design Parameters and of the Working Conditions on the Global Characteristics of a Squeeze Film Damper," *Proc. World Tribol. Cong*., Washington DC, p 287-288

[7] Adiletta, G., Della Pietra, L., 2006, "Experimental Study of a Squeeze Film Damper with Eccentric Circular Orbits," J. Tribol., **128**(2), 2006, pp. 365-377

[8] Diaz, S., and San Andrés, L **,**1999, "Method for Identification of Bearing Force Coefficients and its Application to a Squeeze Film Damper with a Bubbly Lubricant Tribol. Trans., 42(4), , p 739-746

[9] Rice, H.J., Fitzpatrick, J.A., 1991, "Procedure for the Identification of Linear and Non-Linear Multi-Degree-of-Freedom Systems," J. Sound Vib., **149**(3), pp. 397-411

[10] Fitzpatrick, J. A., and Rice, H. J., 1988, "Simplified Partial Coherence Functions for Multiple Input/Output Analysis," J. Sound Vib.,**122**(1), pp. 171-174

[11] Rouvas, C., Murphy, B. T., and Hale, R. K., 1992, "Bearing Parameter Identification Using Power Spectral Density Methods," ImechE, **C432**, pp. 297-302.

[12] Rice, H. J., and Xu, K. Q., 1996, "Linear Path Identification of General Non-Linear Systems," Mech. Syst. Signal Process., **10**(1), pp. 55-63.

[13] Adams, D. E., and Allemang, R. J., 2000, " A Frequency Domain Method for Estimating the Parameters of a Non-linear Structural Dynamic Model Through Feedback," Mech. Syst. Signal Process., **14**(4), pp. 637-656.

[14] Yang, C., Adams, D. E., and Ciray, S., 2005, "System Identification of Non-linear Mechanical Systems Using Embedded Sensitivity Functions," J. Vib. Acoust. , **127**(6), pp. 530-541.

[15] Yang, C., Adams, D. E., and Yoo, S. W., 2003, " Diagnosing Vibration Problems with Embedded Sensitivity Functions," J. Sound Vib., **37**(4), pp. 12-17.

[16] San Andrés, L., and Aguilar, R., 2000, "Leakage and Dynamic Response of a Hybrid Brush Seal-Gas Damper Seal," TRC-SEAL-3-00, Research Progress Report, Texas A&M

University

[17] San Andrés, L., and Delgado, A., 2007, “Parameter Identification of an End Sealed SFD Part II: Improved Predictions of Added Mass Coefficients for Grooved SFDs and Oil Seals,” TRC report, TRC-SFD-2-07, May.

[18] Zeidan, F.Y., San Andrés, L., and Vance, J. M., 1996, “Design and Application of Squeeze Film Dampers in Rotating Machinery,” *Proc. 25th Turbomachinery Symposium*, Houston, TX, pp.169-188.

[19] San Andrés, L., and Delgado, A., 2006, “Identification of Force Coefficients in a Squeeze Film Damper with a Mechanical End Seal- Centered Circular Orbit Tests,” ASME Paper No. IJTC2006-12041 (accepted for publication in ASME J. Tribol.)

[20] Diaz, S., and L. San Andrés, 2001, "Air Entrainment Versus Lubricant Vaporization in Squeeze Film Dampers: An Experimental Assessment of their Fundamental Differences,” ASME J. Eng. Gas Turbines Power, **123**(4), pp. 871-877.

[21] Zeidan, F, and Vance, J., 1990, “ Cavitation Regimes in Squeeze Film Dampers and Their Effect on the Pressure Distribution,” STLE Tribol. Trans., **33**(3), pp. 447-453

[22] San Andrés, L., 2006, “ Tribology Group,” Texas A&M University, http://phn.tamu.edu/TRIBGroup/proj_SFD_air_ing.htm (accessed on 05/15/07)

Appendix A Identification of dry friction force (dry system tests)

The mechanical seal dry friction force is obtained from circular orbit tests without any lubricant in the system. The system is excited with two constant load levels (66, 78 N) for six frequencies (20-35 Hz). Figure A1 depicts the excitation force and displacement orbit at 28 Hz.

Following the procedure described in [3], the energy dissipated by the system is equated to the input work. Figure A2 shows the energy dissipated by the identified residual damping (C_{rv}) and dry friction force (F_{μ}), and the work input into the system.

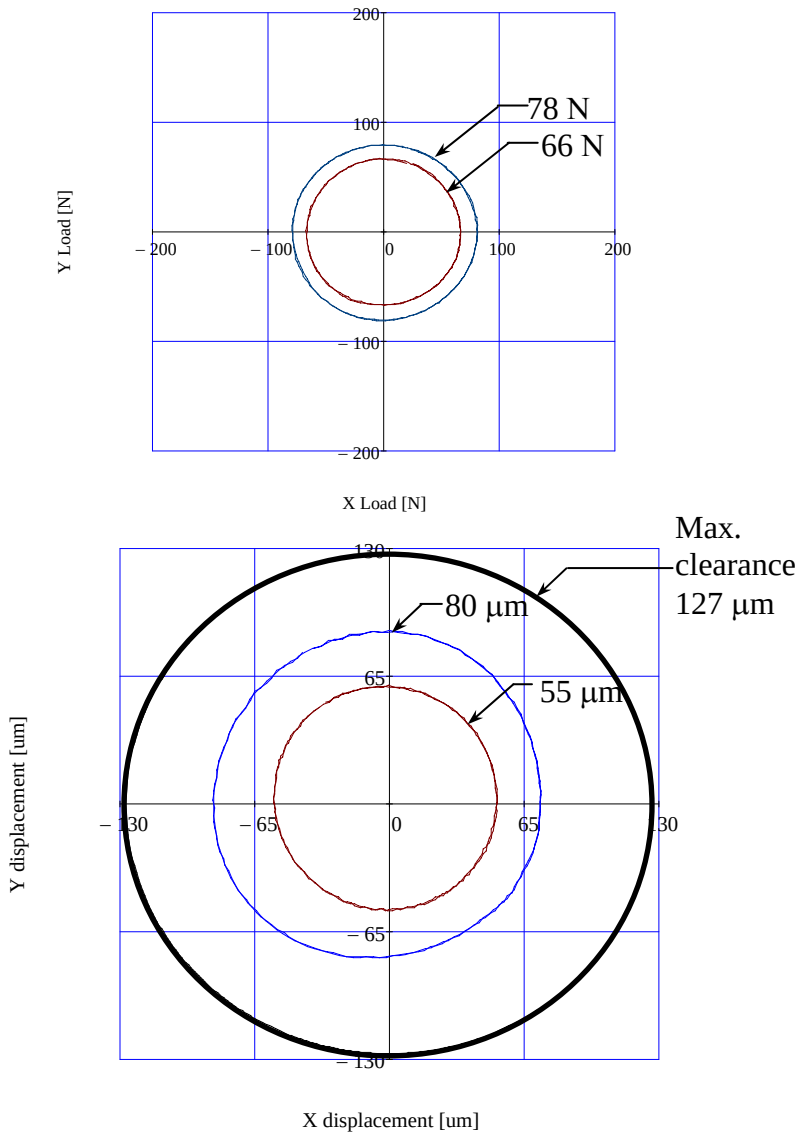

Figure A 1 Recorded load and ensuing displacement orbits for two amplitude load levels. Clearance circle noted. (28 Hz, dry SFD, CCO)

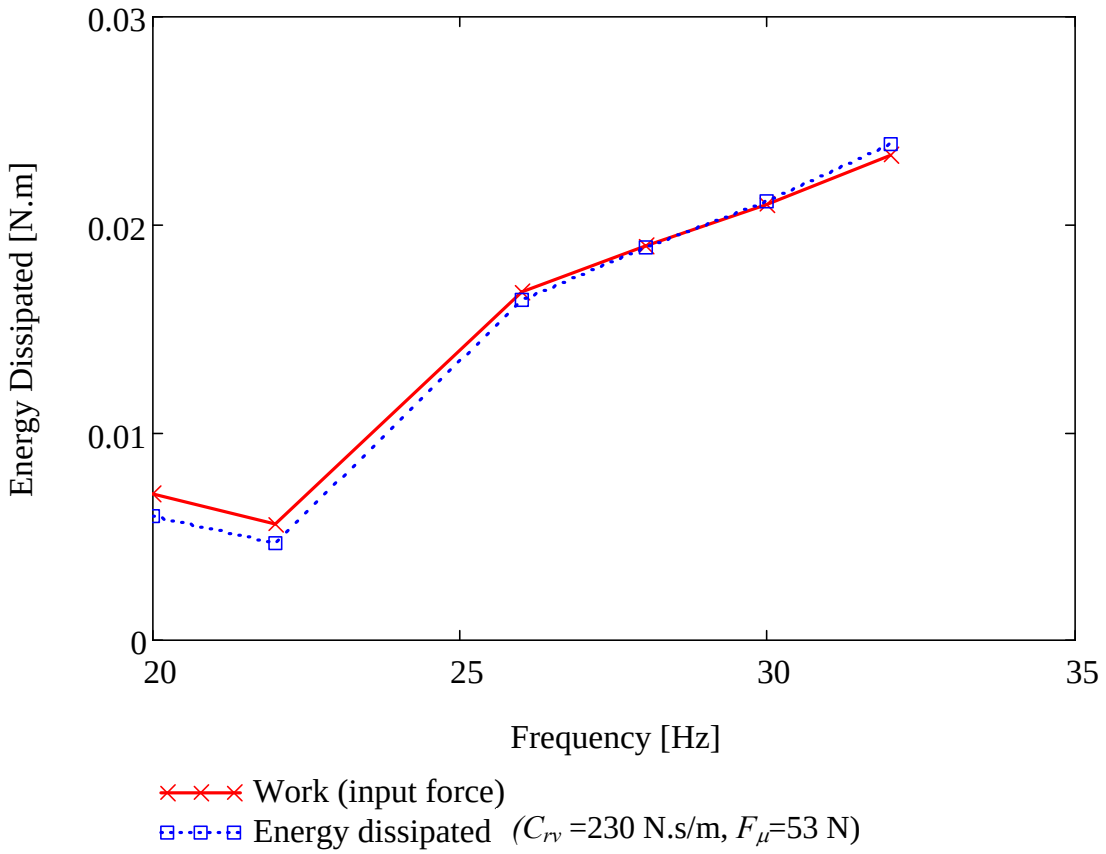

Figure A 2 Work exerted by input force (= dissipated energy) estimated from combined damping model [3]. (Dry system tests)